Geophysical Journal International

Geophys. J. Int. (2011) **185,** 1417–1430 doi: 10.1111/j.1365-246X.2011.05018.x

Hellenic Unified Seismological Network: an evaluation of its performance through SNES method

Antonino D'Alessandro,[1] Dimitris Papanastassiou[2] and Ioannis Baskoutas[2]

[1] *Istituto Nazionale di Geofisica e Vulcanologia, Centro Nazionale Terremoti, Geophysical Observatory of Gibilmanna (OBS Lab), Contrada Gibilmanna, C.P.* 176-90015 *Cefalù (Palermo), Italy. E-mail: antonino.dalessandro@ingv.it*

[2] *Institute of Geodynamics, National Observatory of Athens, Thissio,* 11810 *Athens, Greece*

Accepted 2011 March 14. Received 2011 March 14; in original form 2010 August 26

SUMMARY

In this paper, we analyse the location performance of the Hellenic (Greek) Unified Seismological Network (HUSN) by Seismic Network Evaluation through Simulation method (SNES).

This method gives, as a function of magnitude, hypocentral depth and confidence level, the spatial distribution of the: number of active stations in the location procedure and their relative azimuthal gaps and confidence intervals in hypocentral parameters regarding both the geometry of the seismic network and the use of an inadequate velocity model.

Greece is located on a tectonically active plate boundary at the convergence of the Eurasian and African lithospheric plates and exhibits a high level of seismicity. The HUSN monitors the seismicity in Greek territory from 2007. At present it is composed by 88 seismic stations appropriately distribute in the area of Greece.

The application of the SNES method permitted us to evaluate the background noise levels recorded by the network stations and estimate an empirical law that links the variance of *P* and *S* traveltime residuals to hypocentral distance. The statistical analysis of the *P* and *S* traveltime residuals allowed us to assess the appropriateness of the velocity model used by the HUSN in the location routine process.

We constructed SNES maps for magnitudes (M_L) of 2, 2.5 and 3, fixing the hypocentral depth to 10 km and the confidence level to 95 per cent. We also investigated, by two different vertical sections, the behaviour of the errors in hypocentral parameters estimates as function of depth. Finally, we also evaluated, fixing the hypocentral depth to 10 km and the confidence level to 95 per cent, the Magnitude of Completeness.

Through the application of the SNES method, we demonstrate that the HUSN provides the best monitoring coverage in western Greece with errors, that for $M_L = 2.5$, are less than 2 and 5 km for epicentre and hypocentral depth, respectively. At magnitude 2.5, this seismic network is capable of constraining earthquake hypocentres to depths of about 160 km and more, and provides a threshold of completeness down to magnitude 2 for most of Greek territory.

We delineate some seismogenic areas of southern Greece that probably are not adequately covered by HUSN. Use of the SNES technique could optimize upgrades of the network in these areas.

Key words: Probability distributions; Seismicity and tectonics; Seismic attenuation; Site effects; Computational seismology; Europe.

INTRODUCTION

Seismic networks are powerful tools for understanding active tectonic processes in a monitored seismically active region. Their numerous applications, from monitoring seismicity to characterizing seismogenic volumes, make seismic networks essential tools for assessing seismic hazard in active regions. An appropriately configured seismic network is also a valuable tool for the study of deep geological structures using seismic tomography. The ability to detect small and medium sized events requires a seismic network with sufficient number of optimally distributed, low-noise stations. It is important to assess existing network capabilities to identify seismogenic areas that are not adequately covered, and to quantify measures that will allow network improvement.

Greece is located on a tectonically active plate boundary at the convergence of the Eurasian and African lithospheric plates. The compressional motion between Europe and Africa causes the subduction of the eastern Mediterranean lithosphere to form the

Hellenic Arc and Trench (Papazachos & Comninakis 1971; Comninakis & Papazachos 1972; Makris 1973; Mercier 1977; McKenzie 1978; Dewey & Sengor 1979; Makropoulos & Burton 1984). The tectonic processes that occur in the subducting slab in the Aegean area control the distribution of both seismicity and volcanism (Karagianni *et al.* 2002, 2005). Due to its geodynamic context Greece is the most seismically active region in Europe with consequent high seismic hazard (Tsapanos 2008 and reference contained therein). More than 60 per cent of the European seismicity is expected to occur in this region with earthquake magnitude up to $M_W = 8.2$ (Papazachos 1990).

Four seismological centres monitor Greek seismicity: the Institute of Geodynamics and the Seismological Laboratories of the Universities of Athens, Thessaloniki and Patras.

The Institute of Geodynamics, National Observatory of Athens (IG), is one of the oldest institutes in Greece, operating continuously since 1893. From 1964, the initial network grew in size and extent, so that today it consists of 35 digital telemetric stations installed over the whole country plus seven stations from international agencies cooperating with IG located in the southern Aegean and Crete.

The Seismological Laboratory of the University of Athens belongs to the Department of Geophysics and Geothermy of the National and Kapodistrian University of Athens. The Laboratory first operated in 1929. Today operates 20 stations organized in three digital telemetric networks: CORNET, VOLNET and ATHENET in the areas of the gulf of Corinth, central Greece and around Athens in an area of 100 km radius.

The Laboratory of Geophysics of the Aristotle University of Thessaloniki was established in 1976. Today, the telemetric seismological network of the Laboratory of Geophysics consists of 28 stations. The stations are installed in northern Greece as well as in the north Aegean and Ionian sea.

The University of Patras Seismological Laboratory started operating in 1990. The Patras Seismological Lab Seismic Network (PATNET) covers the wider western Greece area and the Peloponnese. It consists of 21 stations.

In the beginning of 2005, a national project was launched, named: 'Hellenic Unified Seismological Network—HUSN', financed by the Ministry of Development (EPAN 4.5) that intended to unify the Seismological networks of the Greek Institutions, which by the end of 2007, began to give the first results.

In this paper, we apply the Seismic Networks Evaluation through Simulation (SNES) method to the Hellenic Unified Seismological Network (HUSN, as it was at the end of June 2010), which monitors seismicity in Greek territory since 2007. This project made possible the successful interconnection of the seismological networks of the four Institutions for more detailed and precise recording of the seismic activity of the broader area of Greece, the unified calculation of seismic parameters, the publication of common announcements of the occurrence of strong earthquakes, the compilation of a national bulletin of earthquakes and more generally the qualitative upgrading of seismological data and seismological research.

All the signals, from the agreed stations of the partners, are collected by the IG in its central facilities at Thissio in Athens and are retransmitted to all partners, so that everyone receives signals from the rest of the partners. This procedure takes place in real time. At present, 88 digital signals are gathered by IG (Table 1 and Fig. 1), 37 belong to the IG, 23 from Thessaloniki, 13 from Patras, 8 from Athens and 7 from the international agencies cooperating with IG. The staff of IG routinely analysed the data in detail, producing a daily report of located earthquakes in the broader area of Greece and produce a monthly bulletin. The earthquake listings are distributed regularly to several Seismological centres and Universities, as well as to different Organizations and Libraries all over the world. The configuration of the HUSN continues to evolve as contributing Institutions add more stations. Additional information about HUSN is given at http//bbnet.gein.noa.gr.

METHOD

The methods so far proposed to evaluate the performance of a seismic network (Rydelek & Sacks 1989; Sereno & Bratt 1989; Gomberg 1991; Wiemer & Wyss 2000; Marsan 2003; Woessner & Wiemer 2005; Amorèse 2007, Schorlemmer & Woessner 2008) are based on the estimation of the Magnitude of Completeness (M_C) which is defined as the lowest magnitude of events that at least four stations of a seismic network is able to detect (Rydelek & Sacks 1989; Schorlemmer & Woessner 2008).

M_C parameter can be estimated in different ways and using different type data. For example, deviation from the Gutenberg–Richter law earthquake frequency–magnitude distribution (Wiemer & Wyss 2000; Cao & Gao 2002; Marsan 2003; Woessner & Wiemer 2005; Amorèse 2007), changes between the day and nighttime sensitivity of networks (Rydelek & Sacks 1989), comparison of amplitude–distance curves and the signal-to-noise ratio (Sereno & Bratt 1989), amplitude threshold studies (Gomberg 1991; Kvaerna *et al.* 2002) and detection probabilities estimate for each seismic station (Schorlemmer & Woessner 2008). Papanastassiou (1989) by using a similar procedure with the latter example estimated the performance of the seismological network of the IG.

M_C is an important parameter for most studies related to seismicity but it does not give any information about the spatial distribution of expected hypocentral errors. These errors are a function of the accuracy of the velocity model used in hypocentre location and of the geometry, density and noisiness of the stations that make up the network.

For this reason D'Alessandro *et al.* (2011) proposed a new method of analysis called SNES that is used to evaluate the location performance of a seismic network by numerical simulation. The SNES method needs the following input: the location of the stations that make up the network and their noisiness, the velocity model used for hypocentre location routine and a law to estimate the variance in the residual times.

The method gives, as a function of magnitude, hypocentral depth and confidence level: the spatial distribution of the number of active stations in the location procedure, the azimuthal gaps and confidence intervals in hypocentral parameters regarding both the geometry and noisiness of the seismic network, and the appropriateness of a velocity model.

The SNES method is divided into the following five steps:

(1) estimate the average noise power of the vertical component for each station of the seismic network;

(2) estimate the empirical laws that bind the variance of the residual time of *P* and *S* phases to the hypocentral distance;

(3) simulate earthquakes with hypocentres at the nodes of a regular grid covering the area of investigation and calculate the seismic spectra at the stations taking into account propagation effects;

(4) determine the ratio between the earthquake signal and noise spectra, which identifies seismic stations that supply useful information for the hypocenter locations and

(5) construct the covariance matrices of the data and also of the partial derivatives of the model and from these, the covariance matrices of the hypocentral parameters.

Table 1. List of the seismic stations of the HUSN. Codes HL, HT, HA and HP stand for the stations belonging to the Institute of Geodymanics, and the Universities of Thessaloniki, Athens and Patras, respectively. GVD, KARN LAST, SANT, SIVA, ZKR and IDI are stations belonging to international agencies (GEOFON and MEDNET) cooperating with IG.

Code	Latitude	Longitude	Altitude	Inst.	Code	Latitude	Longitude	Altitude	Inst.
PDO	38.5986	21.1833	227	HP	KSL	36.15	29.5833	100	HL
KLV	38.0437	22.1504	758	HL	KFL	38.1096	20.788	264	HP
DRO	37.9522	21.7111	471	HP	KNT	41.162	22.898	380	HT
MAKR	39.0132	22.1317	532	HA	KYTH	36.28	23.036	458	HL
SFD	37.2512	21.0165	45	HP	KZN	40.3033	21.782	791	HL
AMT	37.5324	21.7089	482	HP	LAST	35.1611	25.4786	870	HL
SKIA	39.1665	23.4661	325	HA	LIA	39.8972	25.1805	67	HL
ERET	38.4423	23.8064	810	HA	LIT	40.1003	22.4893	568	HT
DYR	36.7622	22.3337	428	HP	LKR	38.6495	22.9988	185	HL
VLY	37.8524	23.7942	256	HL	LOS	39.933	25.081	460	HT
NAIG	37.7585	23.4887	221	HL	LTK	38.0228	22.9673	408	HP
XRY	34.8748	25.6943	21	HL	MEV	39.785	21.229	1500	HT
NEST	40.4147	21.0489	1056	HT	NEO	39.3056	23.2218	510	HL
NIS1	36.6023	27.1782	378	HT	NISR	36.6106	27.1309	48	HL
LKD2	38.7889	20.6578	485	HT	NVR	41.3484	23.8651	627	HL
KAVA	40.9941	24.5119	95	HT	OUR	40.334	23.982	60	HT
DSF	38.4112	22.5271	701	HP	PAIG	39.9363	23.6768	213	HT
GUR	37.9363	22.3423	1080	HP	PLG	40.3714	23.4438	590	HL
EFP	38.4269	21.9058	135	HP	PRK	39.2456	26.2649	130	HL
KALE	38.3911	22.1398	760	HA	PTL	38.0473	23.8638	500	HL
LAKA	38.2401	21.9785	505	HA	RDO	41.145	25.5355	116	HL
ATHU	37.9665	23.7845	308	HA	RLS	38.0558	21.4647	97	HL
PYL	36.8955	21.742	220	HP	SANT	36.371	25.459	540	HL
SIGR	39.2114	25.8553	92	HT	SIVA	35.0175	24.81	95	HL
AGG	39.0211	22.336	622	HT	SMG	37.7042	26.8377	348	HL
ALN	40.8957	26.0497	110	HT	SOH	40.8206	23.3556	728	HT
AOS	39.17	23.88	200	HT	SRS	41.1086	23.5846	321	HT
APE	37.0727	25.523	608	HL	THE	40.6319	22.9628	124	HT
ARG	36.2135	28.1212	148	HL	THL	39.5646	22.0144	86	HL
ATH	37.9738	23.7176	93	HL	VAM	35.407	24.1997	225	HL
CHOS	38.3868	26.0506	854	HT	VLI	36.718	22.9468	220	HL
DID	37.5063	23.2368	525	HP	VLS	38.1768	20.5886	402	HL
EVR	38.9165	21.8105	1037	HL	VLX	37.3703	22.3793	1031	HP
FNA	40.7818	21.3835	750	HT	XOR	39.366	23.192	500	HT
GRG	40.9558	22.4029	600	HT	ZKR	35.1147	26.217	270	HL
GVD	34.8392	24.0873	180	HL	ACOR	37.8902	22.8692	437	HA
HORT	40.5978	23.0995	925	HT	VILL	38.1642	23.3122	650	HA
IDI	35.288	24.89	750	HL	SMTH	40.4709	25.5304	365	HL
IGT	39.5315	20.3299	270	HT	PSA1	38.3253	21.8837	3	HL
ITM	37.1787	21.9252	423	HL	IACM	35.3058	25.0709	45	HL
JAN	39.6561	20.8487	526	HL	ANKY	35.867	23.3012	143	HL
KARN	35.4019	23.9174	420	HL	MHLO	36.6898	24.4017	175	HL
KARP	35.5471	27.161	524	HL	ZKS	37.6969	20.7853	374	HL
KEK	39.7127	19.7962	227	HL	NPS	35.2613	25.6103	288	HL

More details about the method and the computation algorithms can be found in D'Alessandro *et al.* (2011). In this paper, we apply the SNES method to the HUSN, to estimate the background noise levels, assess the appropriateness of the velocity model used in location routine, evaluate the hypocentre location uncertainty and determine the M_C with the actual seismic network configuration (as it existed at the end of 2010 June).

CHARACTERIZATION OF THE SEISMIC NOISE

The location performance of a seismic network is strongly affected by the background noise levels affecting its stations. Indeed, precise reading of the seismic phases depends on the quality of the signal to be analysed in the frequency range typical of regional events, or on its Wideband Spectral Ratio (WSR). For an accurate picking of P_g and P_n phases, a WSR > 10 is needed; below this threshold the error in picking the first phase is strongly controlled by the WSR, whereas above this threshold it is independent (Zeiler & Velasco 2009). Zeiler & Velasco (2009) have empirically verified that the error in picking of seismic phases for WSR > 10 was approximately 0.1 s.

The noise level of a seismic station is generally investigated using the Power Spectral Density (PSD) of the acceleration signal; the noise level is dependent on the quality of the recording vault installation and on the intrinsic noise of the site.

We estimated the mean acceleration PSDs of the vertical component of the noise for all stations of the HUSN using PQLX software (McNamara & Buland 2004). For almost all the PSDs the noise recorded in the time period 2007–2010 was used.

Fig. 1 shows the estimated power of the seismic noise for HUSN stations. We derive this by calculating the mean of the vertical

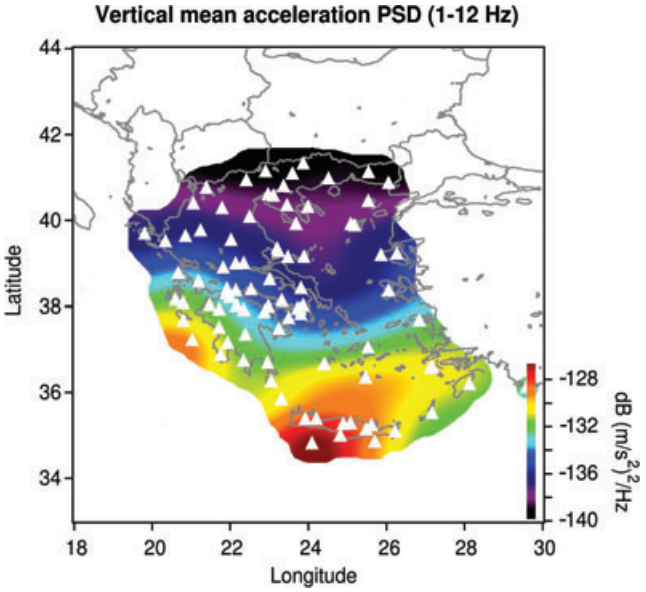

Figure 1. Map of the average power of the vertical component of the noise for HUSN, stations configuration as of 2010 June. This was derived by calculating the mean of the vertical component of the acceleration PSD, in the frequency range 1–12 Hz, for each station and applying the inverse distance weighted method for the standardization of the data grid. A 2-D moving average was applied to the grid to eliminate local effects possibly related to bad installation and also to highlight regional scale trends in background noise.

component of the acceleration PSD, in the frequency range 1–12 Hz, for each station and applying the inverse distance weighted method (Shepard 1968) for data grid standardization. We applied a 2-D moving average to the grid to minimize local effects related to possible bad installations and to emphasize the presence of regional scale noise characteristics. Characterization of the seismic noise and construction of a mean seismic noise power map can help technicians identify stations with anomalous noise levels. Comparison of noise levels shown on such a map and those determined for a possible new site may allow rejection of a site with high local noise problems.

The noise power map in Fig. 1 shows areas of high seismic noise in the Greek Volcanic Arc with maximum at Crete Island whereas very low noise is present in the rest of Greece.

The high noise level at the Greek Volcanic Arc is probably a sum of three main effects: geographical position, geology and volcanic activity. Seismic stations near coast or on islands are generally characterized by high level of seismic noise (McCreery *et al.* 1993). The presence of Quaternary sedimentary rocks can give rise to resonance phenomena and consequently to the amplification of motion at the surface. Finally, the volcano-seismic activity, characterized by periods of volcanic tremors and seismo-volcanic activity (Soloviev *et al.* 1992; Hatzfeld *et al.* 1993; Bohnhoff *et al.* 2006) makes this area very noisy.

ESTIMATION OF THE RESIDUAL TIME VARIANCES OF THE SEISMIC PHASES

An earthquake is identified either by its hypocentral parameters, which are the origin time T_0 and the position (x_0, y_0, z_0), and by the associated uncertainties $(\sigma_T, \sigma_x, \sigma_y, \sigma_z)$. Hypocentral parameters are determined by inversion of the arrival times of seismic phases read on seismograms recorded by stations that make up the seismic network. The best estimate of the focal parameters is typically determined in an iterative mode by minimizing the Euclidean norm of the residual traveltimes ΔT, assuming you know the velocity model of the Earth

$$\Delta T = T_{\rm obs} - T_{\rm cal}, \tag{1}$$

where $T_{\rm obs}$ is the time read on the seismogram, $T_{\rm cal}$ is the calculated traveltime. The error in reading the seismic phase can be considered random, so the statistical study of the sign of ΔT, on seismic rays that have traversed the same volume, can provide information about the existence of regions with above (+) or below (−) average speeds than those of the Earth model used.

Assuming the absence of systematic errors introduced by the velocity model or by the seismic phase readings, the uncertainties on estimated hypocentral parameters depend mainly on the variance of the residual times. The variance of the residual times $\sigma^2_{\Delta T}$ is a function of both WSR ($\sigma^2_{\rm WSR}$) and the velocity model uncertainness used in the inversion procedures ($\sigma^2_{\rm MOD}$). Assuming the statistical independences of $\sigma^2_{\rm WSR}$ and $\sigma^2_{\rm MOD}$

$$\sigma^2_{\Delta T} = \sigma^2_{\rm WSR} + \sigma^2_{\rm MOD}. \tag{2}$$

For WSR values >10, in the frequency range 0.1–10 Hz, the variance $\sigma^2_{\rm WSR}$ in the reading of seismic phases $P_{\rm g}$ and $P_{\rm n}$ is very small and takes on values close to 0.01 s^2 (Zeiler & Velasco 2009). However, it has been experimentally observed that the variance of the residual time $\sigma^2_{\Delta T}$ typically takes much larger values and this difference is obviously attributed to the second term of (2). The variance $\sigma^2_{\rm MOD}$ introduced by the use of a velocity model that inadequately characterizes the geological complexity of the area, can take quite high values; the greater the value, the less adequately the model is inadequate represents the local geology. So $\sigma^2_{\Delta T}$ can be attributable to inappropriateness of the velocity model used in hypocentre location routine or to velocity anisotropy (Rothman *et al.* 1974).

The experimental separation of the two terms of (2) may be difficult to implement. In this work, we have estimated an empirical law that binds the variance of residual time to hypocentral distance. To this end, *P* and *S* seismic phases were used for the earthquakes located by the HUSN between 2007 and 2010 to create two different residual time databases versus hypocentral distance. We used the databases, consisting of a total of more than 420 000 residual time-hypocentral distance pairs, to construct the 2-D colour histograms of Fig. 2. For their construction, we used classes of 0.1 s for the residual time and 10 km for hypocentral distances.

For each distance class, we calculated the variance of the residual times to maximum hypocentral distances of 650 and 440 km for *P* and *S* phases, respectively, beyond which lack of data made the statistical estimates insignificant.

We fitted the data variance estimates with polynomial functions. The process of choosing the order of the polynomial fitting is critical to the good predictability of the solution, so we used statistical criteria. Indeed, when the polynomial or the complexity increases, the solution shows greater adherence to the observed data but also with the related component of random error.

The way in which the solution behaves in relation to the variation in complexity can be studied through bias and variance: bias quantifies the deviation from the mean estimate of the optimal estimator and variance quantifies the stability of the estimator with respect to the observed data. In general, with increasing complexity, bias decreases whereas variance increases.

To properly balance these two quantities and determine the complexity of the optimal model, we estimated the generalization error

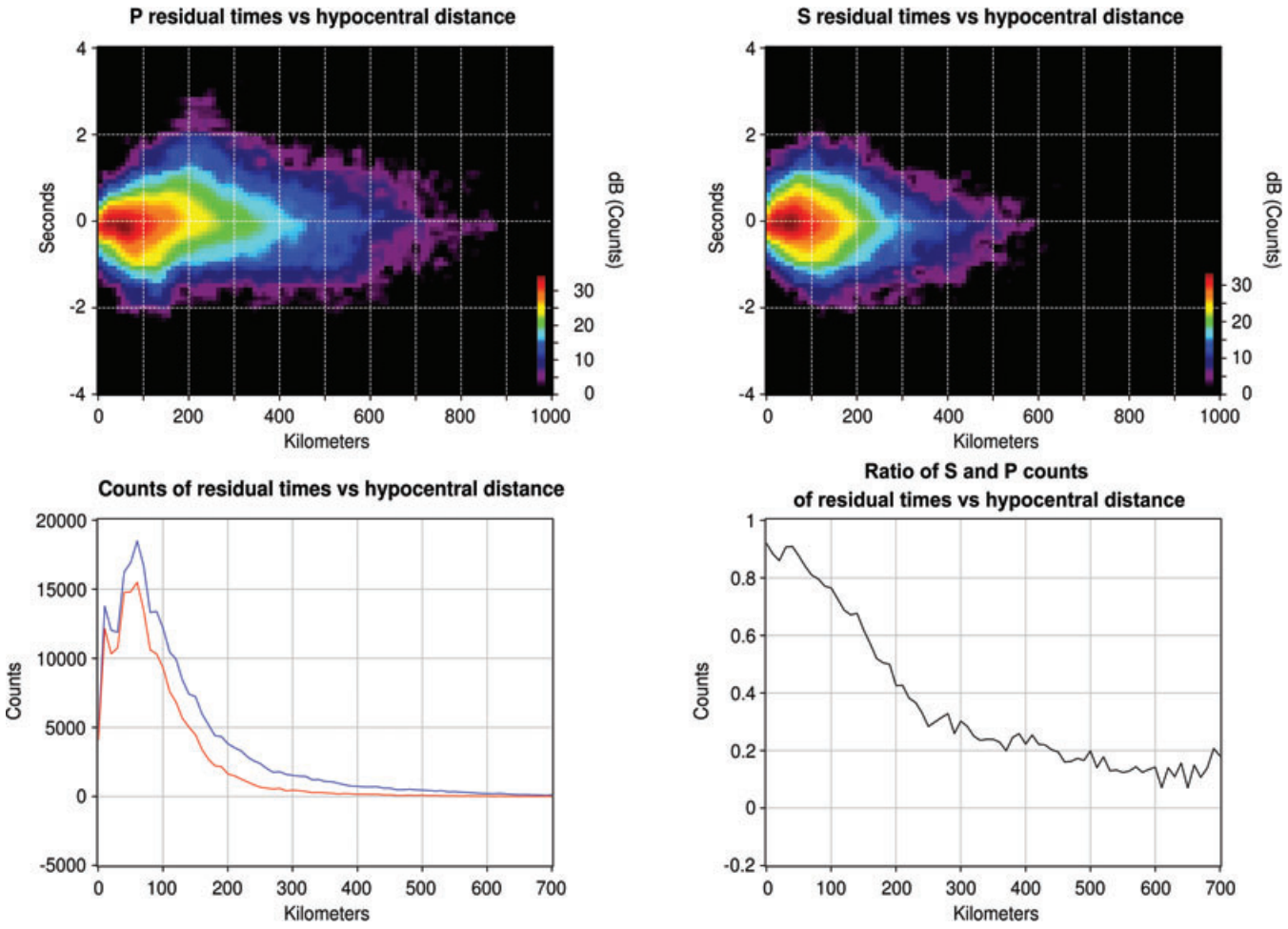

Figure 2. Top, 2-D histogram of *P* and *S* residual time versus hypocentral distance in logarithmic colour scale; below, the number of *P* and *S* residual times (blue: *P* phases residual times, red: *S* phases residual times) from local and regional earthquakes and their ratio. The counts ratio *S*/*P*, shows an inverse relation with hypocentral distance. This ratio assumes the maximum value of 0.92 and decreases falling below 0.2 for hypocentral distances greater than 450 km.

or expected error of prediction. We determined the order of the polynomial so as to minimize this error.

Fig. 2 shows the 2-D histograms of *P* and *S* residual times and its counts and ratios as function of hypocentral distance. The 2-D histograms show about symmetrical shape and little spread. The spread in the residual time histograms can be modelled as the sum of random scatter in the times due to picking errors and systematic traveltime difference due to lateral heterogeneity.

The *P* and *S* phases counts have maximum values between 10 and 100 km with a common local maximum at 60 km. The S/P counts ratio shows an inverse relation with hypocentral distance. This ratio assumes a maximum value of 0.92 that decreases with the hypocentral distance falling below 0.2 for hypocentral distances greater than 450 km. Therefore, at distance less than 200 km the *S* phases contribute significantly to the process of hypocentre location. Using seismic phases with different velocities has the effect of better constraining a hypocentre; so generally, it is advantageous to use as multiple phases for each seismic stations assuming that these are correctly identified.

Fig. 3 shows the mean and variance of *P* and *S* phases residual times as function of hypocentral distance. The average of the *P* phase residual times shows negative value between 0 and 150 km and above 300 km, and have positive values between 150 and 300 km. Probably the *P* velocity model is too slow in its shallow and deep part, while it is too fast in its middle part. On the contrary, the average of the *S* residual times takes negative values for the entire distances interval analysed, especially above 250 km. This behaviour is probably linked to an *S* velocity model that is too fast, especially in its deepest part. The *S* velocity is obtained from the *P* velocity model by dividing by 1.73. Non-zero mean values of the residual times may introduce systematic errors in hypocentre location. For this reason, the *P* and *S* velocity model used in hypocentre location routine need optimization.

Eqs (3) and (4) show the polynomials of fifth order obtained by polynomial regression for the variance in the residual times of the *P* and *S* phases, respectively.

$$\sigma_P^2 = 9.006 \times 10^{-14}x^5 - 7.784 \times 10^{-11}x^4 + 1.851 \times 10^{-8}x^3 - 2.419 \times 10^{-5}x^2 + 2.053 \times 10^{-3}x + 3.056 \times 10^{-2} \quad (3)$$

$$\sigma_S^2 = 1.509 \times 10^{-12}x^5 + 1.356 \times 10^{-9}x^4 + 4.307 \times 10^{-7}x^3 - 5.694 \times 10^{-5}x^2 + 4.580 \times 10^{-3}x + 3.313 \times 10^{-2} \quad (4)$$

and are valid to hypocentral distance of 650 and 440 km,

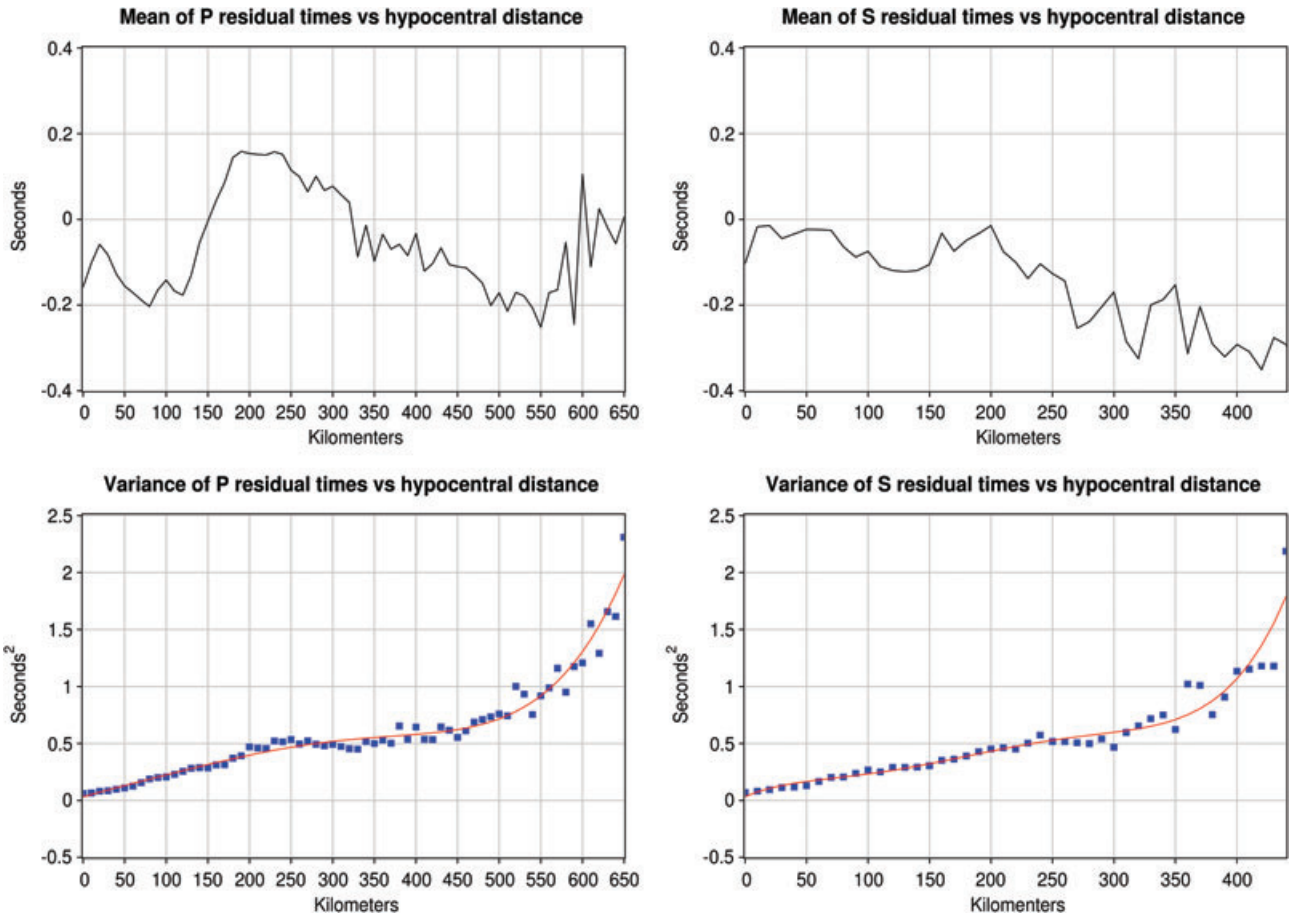

Figure 3. Top, the mean value of *P* and *S* phase residual times as function of hypocentral distance; bottom in blue, the variance of *P* and *S* phase residual times as function of hypocentral distance and in red, the curves obtained from the polynomial regressions (eqs 3 and 4).

respectively. Under the assumption that σ^2_{SNR} assumes a negligible value, the (3) and (4) can be interpreted in terms of σ^2_{MOD}. Fig. 3 shows that both σ^2_P and σ^2_S grow rapidly when the hypocentral distance increases.

The law that describes σ^2_P as a function of hypocentral distance is particularly well described by a fifth-order polynomial function (3). For hypocentral distances of less than about 200 km, the σ^2_P shows almost linear upward trend with slow growth rate. In this distance interval the first arriving seismic phase has travelled within the upper crust. This trend of σ^2_P can be justified by the geological complexity of Greek area and resulting velocity heterogeneity. For hypocentral distances between approximately 200 and 500 km, the variance tends to stabilize around the value 0.6 s^2. In this interval the seismic phase first arrival has travelled primarily in the upper mantle. The behaviour of the σ^2_P in this interval is therefore attributable to the greater homogeneity of the upper mantle compared to the crust. Finally, for hypocentral distances greater than about 500 km σ^2_P begins to grow rapidly. This behaviour is due to the unsuitability, in its deep part, of the 1-D velocity model used by HUSN in the hypocentre location routine and the fact that it does not take into account the effect of the earth curvature.

The law that describes the σ^2_S as a function of hypocentral distance is well described by a fifth-order polynomial function (4). The σ^2_S attains higher values than σ^2_P expecially for hypocentral distance greater than 300 km. The σ^2_S show very similar behaviour to σ^2_P out to 300 km, showing a linear upward trend with slow growth rate but beyond about 300 km it begins to grow exponentially.

We use eqs (3) and (4) to estimate the variance of the residual times for each station. The uncertainty of the phase readings can be described by the covariance matrix $\boldsymbol{C}_d$ where the main diagonal terms are the variances in the estimated residual times for the individual stations, while the off-diagonal terms are the covariances that describe the relationship between errors of station pairs. In this study, we have reasonably assumed that there is no correlation between reading errors made on the arrival times of the different stations and therefore the off-diagonal matrices of $\boldsymbol{C}_d$ are zeros.

EARTHQUAKE SIMULATION: SEISMIC SPECTRA CALCULATION

Once a source model has been defined, it is possible to calculate the spectrum of seismic waves at the focus $\boldsymbol{S}(\omega)$ or the Fourier transform of the impulse produced by the source $\boldsymbol{S}(t)$ that is a function of the parameter that characterized the model.

The amplitude of the seismic spectrum is generally described by complex patterns that are tied to specific functions of directivity. These are a direct consequence of the finite source extension and imply a dependence of the spectrum on the direction of observation. In fact, due to destructive interference of seismic waves emitted by the source, some frequencies cannot be observed and the high frequencies are attenuated by laws of the type $\omega^{-\gamma}$. For these reasons, $\boldsymbol{S}(\omega)$ is often represented in terms of the envelope of mean azimuthal average $\bar{\boldsymbol{S}}(\omega)$ and reported in bi-logarithmic axes.

The main morphological features of the seismic spectrum are described by different models of earthquakes in near-field and far field approximations. Since, in general, the experimental observations are made at hypocentral distances that are much greater than the average size of the seismic sources, far field approximations are used more frequently.

For earthquakes of small and medium magnitude ($M < 6$) the length and width of the fault are comparable ($L \cong W$); for these events Brune's circular fault model (1970) is commonly used. The source model proposed by Brune (1970) consists of a flat circular fault having a finite radius the action of which is a shear stress pulse applied to the whole surface but in the opposite direction on the two inner surfaces of the fault.

The waveform generated at the source is subject, during propagation, to attenuation phenomena that significantly change both the amplitude and the frequency content. Thus, the seismic spectrum $\bar{\boldsymbol{S}}_R(\omega, \boldsymbol{x})$ at a generic receiver of position $\boldsymbol{x}$ will be

$$\bar{\boldsymbol{S}}_R(\omega, \boldsymbol{x}) = \bar{\boldsymbol{S}}(\omega) E(\boldsymbol{x}) A(\omega, \boldsymbol{x}), \tag{5}$$

where $E(\boldsymbol{x})$ is the term that takes into account the attenuation due to the enlargement of the wavefront, the partitioning of energy in the presence of interfaces and free surface effects, which are the only attenuation effects in perfect elastic medium, while $A(\omega, \boldsymbol{x})$ takes into account both energy dissipation due to imperfect elasticity and scattering phenomenon.

In a perfectly elastic medium, wave attenuation is fully described by the geometrical spreading $G(\boldsymbol{x})$, which is compatible with the ray theory and by the partition of energy at the buried interfaces $P(\boldsymbol{x})$ and at the free surface $F(\boldsymbol{x})$

$$E(\boldsymbol{x}) = G(\boldsymbol{x}) P(\boldsymbol{x}) F(\boldsymbol{x}). \tag{6}$$

The imperfect elasticity of rocks and the presence of a small-scale random component in the heterogeneity of the mechanical parameters cause a frequency-dependent attenuation of the wavefield $A(\omega, \boldsymbol{x})$

$$A(\omega, \boldsymbol{x}) = I(\omega, \boldsymbol{x}) S(\omega, \boldsymbol{x}) B(\omega), \tag{7}$$

where $I(\omega, \boldsymbol{x})$ is the attenuation that depends on the rheology of the medium, $S(\omega, \boldsymbol{x})$ is the attenuation due to scattering phenomenum and $B(\omega)$ is the transfer function of the last surface layers of soil under the station.

More details about the computation algorithms can be found in D'Alessandro *et al.* (2011).

The Brune model and the eqs (5)–(7) were used to calculate the seismic spectra. We used the 1-D velocity model employed by HUSN in the earthquake location routine (Herrin *et al.* 1968). It consists of four homogeneous and elastic layers, having 4, 29, 12 and 40 km thicknesses and P velocities of 5.3, 6, 6.88 and 7.9 km s^{-1}, respectively, on a half-space with P velocity of 8.1. The S velocity model is obtained from the P velocity model dividing by 1.73. The values of density and S-wave velocity used in spectra calculation were estimated using the empirical relationships of Brocher (2005).

Three slightly different attenuation laws exist for different region of Greece: for northern Greece Hatzidimitriou (1993) found $Q_c = 60 f^{0.79}$, valid in the frequency range 1.5–12 Hz; for central Greece Baskoutas (1996) found $Q_c = 62 f^{0.83}$, valid in the frequency range 1–12 Hz; for southern Greece, Polatidis *et al.* (2003) found $Q_\beta = 55 f^{0.91}$, valid in the frequency range 0.6–16 Hz. On the basis of this relation, we used the attenuation law $Q_\beta = 59 f^{0.84}$ taking into account a $Q_\alpha / Q_\beta = 1.5$ (Sato *et al.* 2002), while δ equals 0.05 s^{-1} (Anderson & Hough 1984). In this study, hypocentral depths were fixed at 10 km. Moreover, for the calculation of seismic spectra, the values $\alpha = 6.5$ km, $\Delta\sigma = 6$ MPa, $R_P = 0.55$, $V_C = 0.9\,\beta$ and $k = 3.36$ were assigned to the parameters of the formulas above.

Fig. 4 shows the acceleration PSD of P waves, estimated using the velocity model and the attenuation law described above, as a function various magnitude and epicentral distances. The reference acceleration PSDs of the vertical component of noise (NHNM and NLNM, Peterson 1993) are also plotted for comparison. The PSD of acceleration were calculated from seismic spectra using the following formula

$$PSD = 10 \log_{10} \left(\bar{S}_R(\omega, \boldsymbol{x})^2 \right). \tag{8}$$

Fig. 4 illustrates that the signal-to-noise ratio is a function of the seismic event characteristics (mainly magnitude and epicentral distance), the level of noise present at the station and the frequency interval used to calculate this ratio.

ESTIMATION OF THE HYPOCENTRAL PARAMETERS

Traveltimes are generally a non-linear function of the coordinates of the stations, of the focal parameters and of the velocity model of the Earth being used. In matrix notation, the problem of hypocentral location, assuming linearization of the problem by expansion in Taylor series truncated at the first term, can be written as

$$\boldsymbol{d} = \boldsymbol{G} m, \tag{9}$$

where $\boldsymbol{d}$ is the data vector, $\boldsymbol{m}$ the vector of the model parameters and $\boldsymbol{G}$ the matrix of the spatial derivatives of the traveltimes calculated at the hypocentre.

The solution of (9) provides the calculation of the generalized inverse matrix $\boldsymbol{G}^{-g} \times \boldsymbol{G}$ is a matrix of size $N \times 4$ and its inverse coincides with the generalized inverse only when $N = 4$. Generally $N > 4$ and the problem is over-determined; $\boldsymbol{G}^{-g}$ can thus be estimated in terms of least-squares through its Singular Value Decomposition.

Once the inverse matrix $\boldsymbol{G}^{-g}$ has been calculated, the covariance matrix of the solution can then be calculated as

$$\boldsymbol{C}_S = \boldsymbol{G}^{-g} \boldsymbol{C}_d [\boldsymbol{G}^{-g}]^T. \tag{10}$$

Covariance matrix $\boldsymbol{C}_S$ provides the variances and covariances of the time origin T_0 and of the hypocentral coordinates (x_0, y_0, z_0). The uncertainty of the estimation of hypocentral parameters can then be estimated as a confidence interval for a χ^2 distribution with four degrees of freedom. The confidence interval of the generic focal parameter r_{par} at the confidence level of 95 per cent can be estimated as

$$r_{par} = \sqrt{9.488 \times \sigma^2_{par}}, \tag{11}$$

where σ^2_{par} is the variance of the focal parameter being considered and 9.488 is the value of $\Delta\chi^2$ for the confidence level of 95 per cent and four degrees of freedom. The axes of the ellipsoid of confidence were obtained by removing the terms of $\boldsymbol{C}_S$ related to time origin and by representing them in canonical form. To estimate an average error of location we use the Radius of Equivalent Sphere (RES) parameter

$$\mathrm{RES} = \sqrt[3]{r_1 \times r_2 \times r_3}, \tag{12}$$

where r_1, r_2 and r_3 are the semi-axes of the confidence ellipsoid.

It is important to point out that this type of error estimate does not take into account location bias due to systematic model error, so the actual error will generally exceed this estimate.

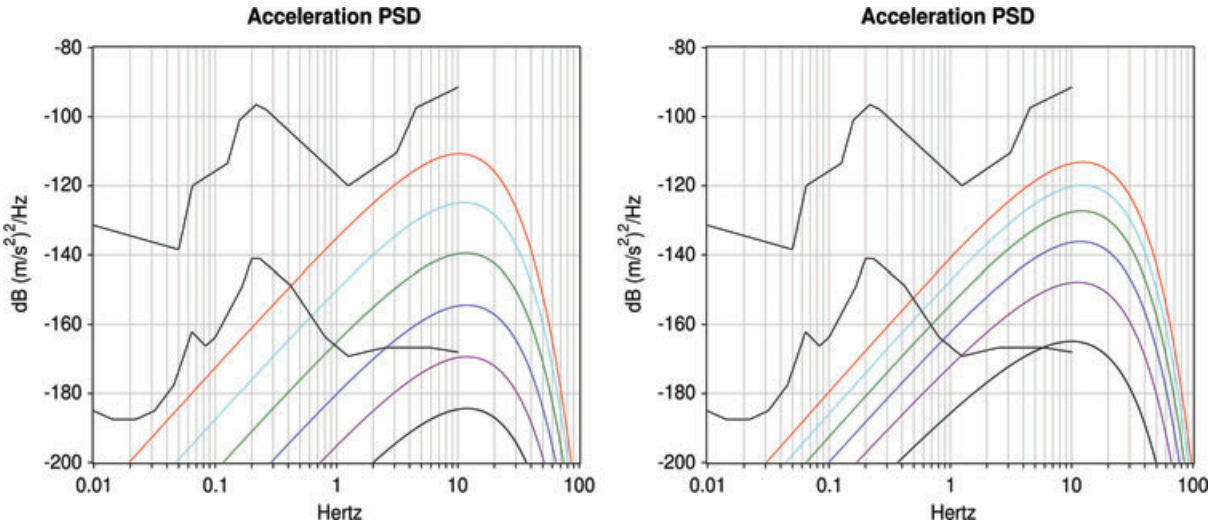

Figure 4. Left, acceleration PSD of *P* waves in decibels calculated by fixing the epicentral distance and varying the magnitude ($\Delta = 100$ km, black: $M_L = 0.5$, purple: $M_L = 1$, blue: $M_L = 1.5$, green: $M_L = 2$, cyan $M_L = 2.5$, red: $M_L = 3$); right, same as left except fixing the magnitude and varying the epicentral distance ($M_L = 2$, black: $\Delta = 320$ km, purple: $\Delta = 160$ km, blue: $\Delta = 80$ km, green : $\Delta = 40$ km, cyan: $\Delta = 20$ km, red: $\Delta = 10$ km). Hypocentral depth fixed at 10 km; for comparison the NHNM and NLNM reference spectra of Peterson (1993) are also shown.

LOCATION PERFORMANCE OF THE HUSN

In this study, we investigated the location performance of the HUSN for magnitudes $M_L = 2$, 2.5 and 3, by fixing the hypocentral depth at $H = 10$ km and the confidence level of the hypocentral parameter estimates at $P = 95$ per cent. For each station we estimated PSD acceleration at 95 per cent of the threshold and used it to calculate WSR in the frequency range 1–12 Hz, which is typical of the seismic phases of regional events

$$\mathrm{WSR}_{(1-12\,\mathrm{Hz})} = 10\log_{10}\left(\frac{\int_1^{12} PSD_E\,df}{\int_1^{12} PSD_S\,df}\right) \tag{13}$$

where PSD_E is the power spectrum of the theoretical *P* phase. For each event, stations with WSR > 10 were declared to be active for hypocentre location.

For each simulated event, after the active stations with useful *P* phases for the location process were identified, the corresponding *S* phases were added only for stations having a better WSR in such proportions as to maintain the average ratio $P_{\mathrm{phasenumber}}/S_{\mathrm{phasenumber}}$ equal to that determined for the seismic catalogue of the HUSN.

We discretized the study area using a square mesh having 5 km sides, while the SNES maps were calculated for amplitude confidence intervals at 95 per cent of the hypocentral parameter estimate. Uncertainties in the focus parameters were represented up to 5 s for the origin times and up to 10 for the epicentre and hypocentral depth. To mitigate the random noise, a 2-D moving average with square windows having 5-points side was applied to the map, followed by application of a cubic 2-D spline interpolation to improve graphics.

Figs 5–7 show SNES maps estimated respectively for $M_L = 2$, 2.5 and 3. Each SNES map is divided into six submaps that report the number of active stations and their azimuthal gaps, and the amplitude of the confidence interval at 95 per cent of the estimated origin time, latitude, longitude and hypocentral depth. The azimuthal gap is a parameter often used to get an indication of the reliability of the epicentral solution. This is defined as the largest gap in azimuth from the event to any two seismic stations. A azimuthal gap of 180° or larger indicated that all the stations are on one side of the event.

Fig. 8 shows instead the main geographic region of Greece, the seismogenic sources of shallow earthquake in Greece and surrounding areas (Papaioannou & Papazachos 2000), the M_C and the hypocentral position uncertainty for $M_L = 2$, 2.5 and 3, $H = 10$ km and confidence level of 95 per cent. The hypocentral position uncertainty maps were calculated as RES of the 95 per cent confidence ellipsoid. Finally, the M_C map was determined by considering only those earthquakes able to activate at least four stations.

The SNES maps show that events with a magnitude of $M_L = 2.0$ are recorded by eight stations at most and the azimuthal gap that does not decrease below 110°; only a small area in the Peloponnese and Central Greece is covered with expected epicentre and hypocentral depth errors of 3 and 5.5 km or less respectively.

For $M_L = 2.5$, the maximum number of stations increases to just over 20 while the minimum azimuthal gap drops to about 50°; with the exception of few areas in Cyclades Islands, most of the Greek territory is well covered for the epicentre estimation with errors of about 3 km or less with a minimum of about 1 km. However, only part of the Western Greece appear covered for the hypocentral depth estimation with errors that never goes below about 4 km.

For $M_L = 3$ the maximum number of stations goes above 45, while the minimum azimuthal gap drops to about 30°; for this magnitude almost the whole Greek territory appear covered for both epicentre and hypocentral depth estimation. While the epicentral errors reach 2 km for almost the area covered by HUSN, the hypocentral depth errors continues to show relatively high values and only for a small area in the western Greece, it go down to 4 km.

From the analysis of the SNES maps, we observe that an increase in magnitude corresponds to an increase in the area covered and in the quality of location. However the minimum error for hypocentral depth does not drop below about 3.5 km also for $M_L = 3$ or above.

The depth is the most difficult hypocentral parameter to determine, particularly for regional events, due to the fact that the travel-time derivative with respect to depth changes very slowly as function

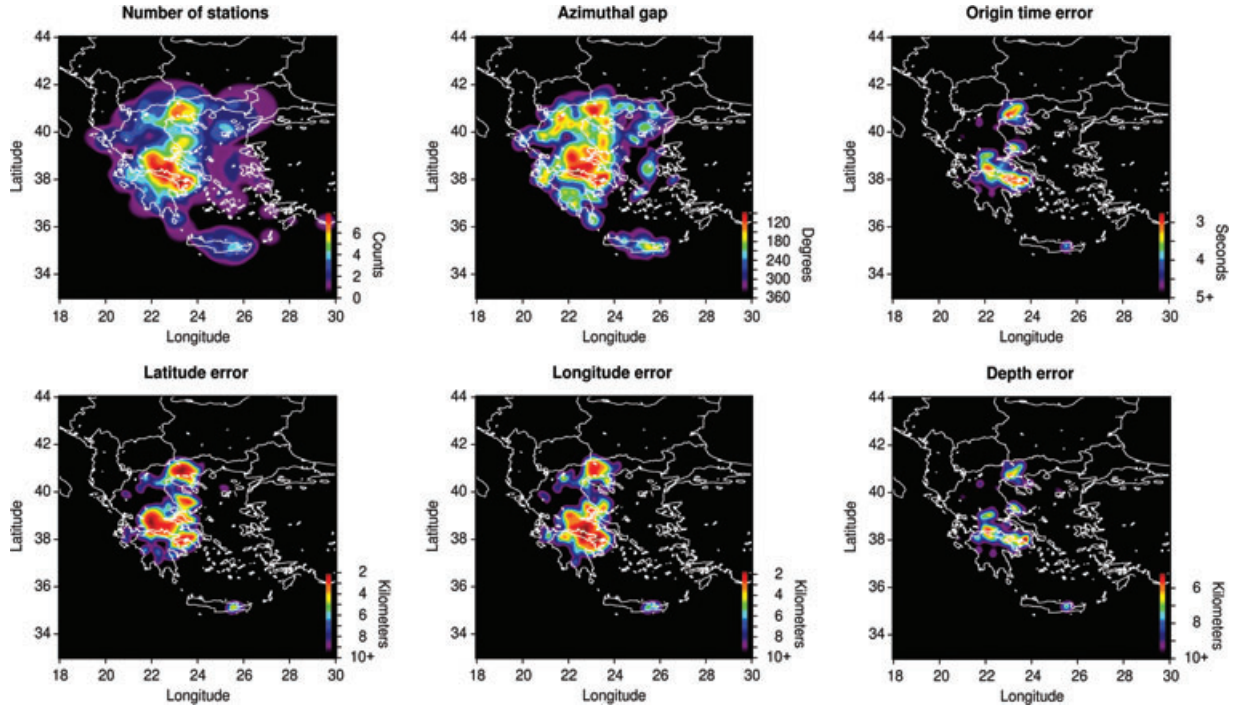

Figure 5. SNES maps for $M_L = 2$, $H = 10$ km and confidence level of 95 per cent. The SNES maps show that events with a magnitude of two are recorded by eight stations at most and the azimuthal gap does not decrease below 110°; only a small area in the Peloponnese and central Greece is covered with expected epicentre and hypocentral depth errors of 3 and 5.5 km or less respectively.

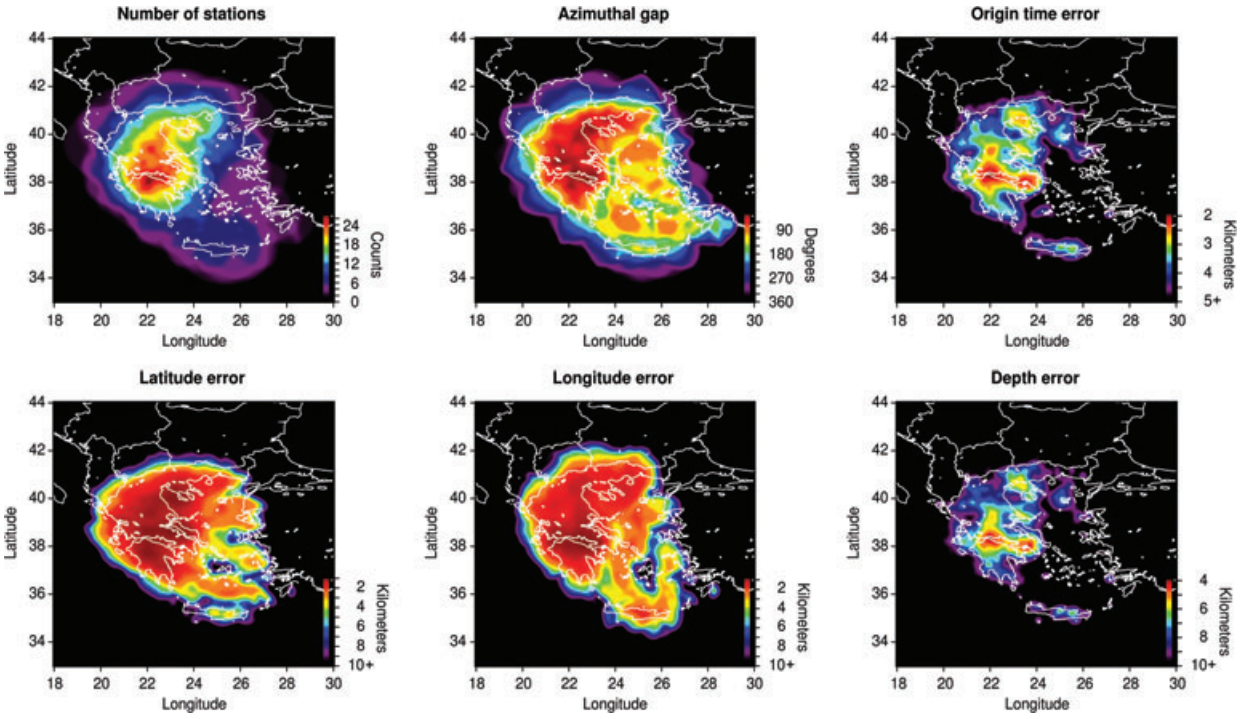

Figure 6. SNES maps for $M_L = 2.5$, $H = 10$ km and confidence level of 95 per cent. For $M_L = 2.5$, the maximum number of stations increases to just over 20 while the minimum azimuthal gap drops to about 50°; with the exception of few areas in Cyclades Islands, most of the Greek territory is well covered for the epicentre estimation with errors of about 3 km or less with a minimum of about 1 km. However, only part of the western Greece appears covered for the hypocentral depth estimation with errors that never goes below about 4 km.

of the depth unless the station is very close to the epicentre. In other words the depth can be moved up and down without much change in the traveltime. The focal depth is well constrain when the phases that are included in the hypocentre location procedure have different sign of the partial derivative such as for very locally observed direct up-going *P*g and down-going *P*n.

The map of the seismogenic sources of shallow earthquake in Greece and surrounding areas of Fig. 9 divides the Greek territory

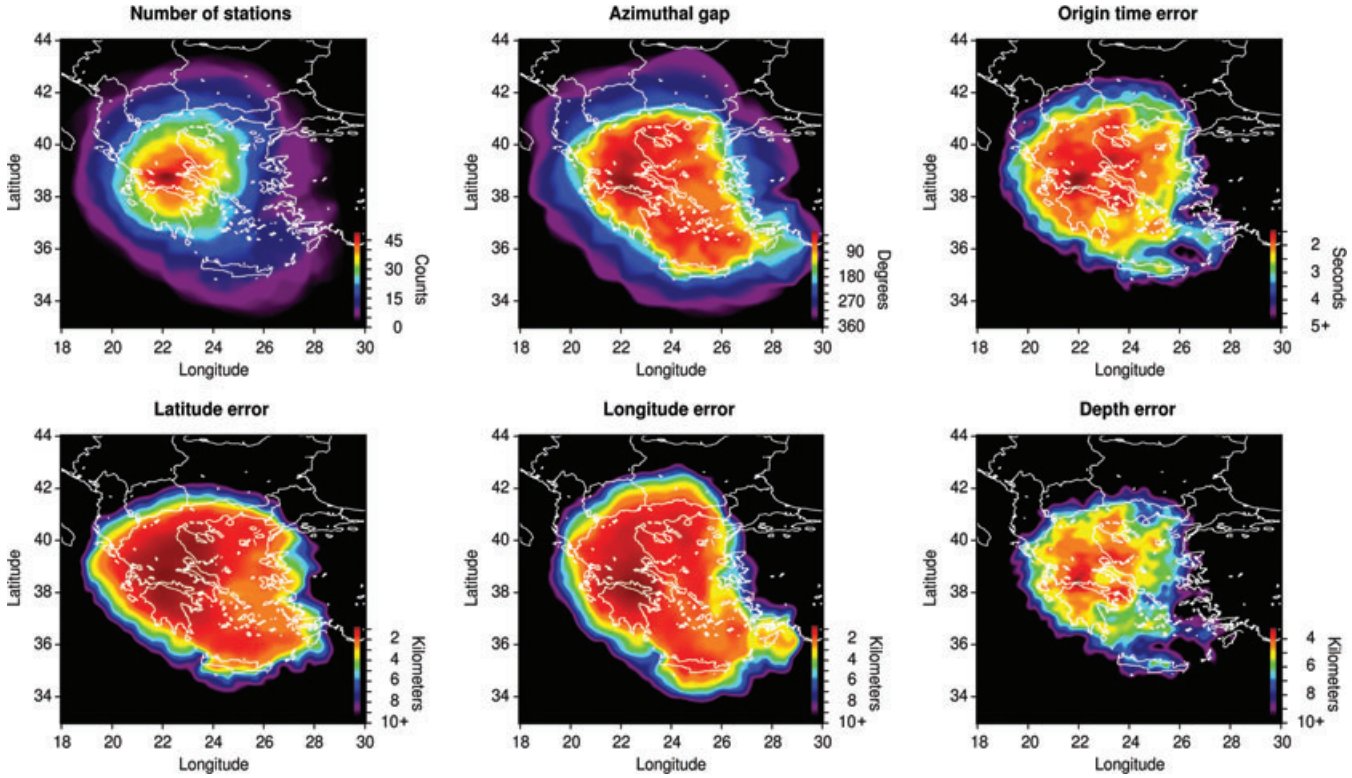

Figure 7. SNES Maps for $M_L = 3$, $H = 10$ km and confidence level of 95 per cent. For $M_L = 3$ the maximum number of stations goes above 45, while the minimum azimuthal gap drops to about 30°; for this magnitude almost the whole Greek territory appear covered for both epicentre and hypocentral depth estimation. While the epicentral errors reach 2 km for almost the area covered by HUSN, the hypocentral depth errors continues to show relatively high values and only for a little area in the Western Greece, it goes down to 4 km.

into 67 zones separated on the basis of seismicity, active tectonics, geological and geomorphological information (Papaioannou & Papazachos 2000). Seismogenic areas of particular significance have been identified by the presence in them of seismogenic sources having a magnitude of $M_{max} > 7$ (Papaioannou & Papazachos 2000) and on the basis of Peak Ground Acceleration (PGA) at 10 per cent probability of exceedance estimated for shallow seismicity and intermediate soil conditions and for an exposure time of 50 yr (Tsapanos *et al.* 2004; Tsapanos 2008).

The seismogenic zones of northern Greece with, the exception of some areas are not covered for $M_L = 2$. However, the main important seismogenic area of Macedonia, number 35, characterized by a predominantly normal faulting mechanism and containing active faults of potential earthquakes of $M_W > 7$, is well covered just for $M_L = 2$. This area, that is characterized by high seismic hazard (PGA $\cong$ 0.25 g), shows for this magnitude a RES < 4.5 km. For $M_L = 2.5$ or larger the all of northern Greece is well covered showing a mean RES < 3 km.

The seismogenic zones of the central Greece and northern Peloponnese (37–45), characterized by a predominantly normal faulting mechanism and containing active faults of potential earthquakes of $M_W > 7$, is well covered just for $M_L = 2$. These zones, characterized by high seismic hazard (PGA $\cong$ 0.30 g), show for this magnitude a RES < 4 km. These zone are the best covered by the HUSN, with a RES that for $M_L = 2.5$ or larger, drop below 2 km.

Except for a small area in Crete, the Greek Islands are not covered for $M_L = 2$. For $M_L = 2.5$, the area covered by HUSN is wide but shows very variable RES in the range 4.4–10 km. The Greek Islands are characterized by different predominant faulting mechanism and contain active faults of potential earthquakes of $M_W > 7$ (14, 15, 16, 28, 47 and 48). Many islands, like Crete, show very high seismic hazard (PGA > 0.35 g). However, the Greek Islands are covered with acceptable errors, only for $M_L = 3$.

The M_C map, reported in Fig. 8, shows that the whole Greek Territory is covered just for $M_L > 2$, with minimum M_C of about 1.6 between the central Greece and the Peloponnese. However, from a comparison with the SNES maps it clearly appears that the parameter M_C significantly overestimates the level of coverage of the HUSN. This parameter simply defines the magnitude of the smallest event that with a certain probability at least four stations of a seismic network can detect. The M_C does not take into account the uncertainty in the hypocentre parameter estimations; this is a function of the velocity model and geometry, density and noise of the stations that make up the seismic network. These results are in a agreement with those recently estimated by Papanastassiou (2011).

Finally Figs 9 and 10 was reported, for $M_L = 2.5$ and confidence level of 95 per cent, two vertical sections of the location uncertainty between points A (40.45N, 19.55E) and A′ (34.12N, 26.73E) and points B (36.57N, 20.95E) and B′ (42.42N, 24.60E).

For the vertical section A–A′, latitude and longitude errors increase with the depth showing minimum values of about 1 km at altitude zero. For this magnitude the epicentres appear well constrained, until the hypocentral depth of about 160 km, for the western part of Greece, and until about 120 km for the eastern part. Fig. 9 shows that latitude and longitude error have a maximum values at about 750 and 550 km, respectively. The error in hypocentral depth shows a very variable value along the vertical section with a minimum value at a depth of about 25 km. Deep earthquakes involve

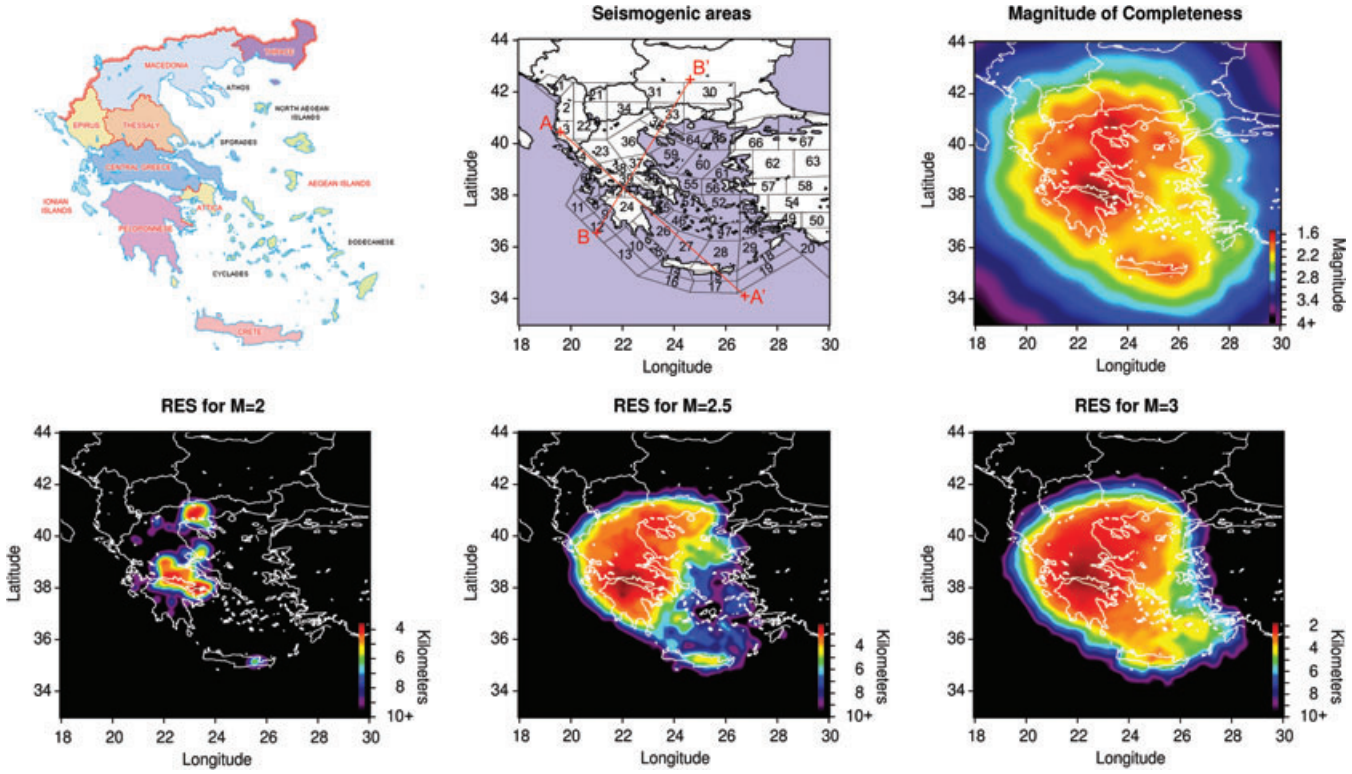

Figure 8. Top: main geographic region of Greece, seismogenic sources of shallow earthquakes in Greece and surrounding areas (Papaioannou & Papazachos 2000) and M_C; bottom: hypocentral position uncertainty map for $M_L = 2$, 2.5 and 3, $H = 10$ km and confidence level of 95 per cent. The hypocentral position uncertainty maps were calculated as RES of the 95 per cent confidence ellipsoid. The M_C map was determined by considering only those earthquakes able to activate at least four stations. The map of seismogenic source also report the SNES vertical section between the points A (40.45N, 19.55E) and A′ (34.12N, 26.73E) and B (36.57N, 20.95E) and B′ (42.42N, 24.60E). For small magnitude earthquakes ($M_L = 2$) only two little areas in Macedonia and between the central Greece and Peloponnese are covered while for slightly larger magnitude earthquakes ($M_L = 2.5$) about the whole western Greek territory is covered with minimum RES value of about 2.5 km. For medium magnitude earthquake ($M_L = 3$) the all Greece is well covered with minimum RES value of 2 km. The M_C map shows that all Greece is covered just for $M_L > 2$, with minimum M_C of about 1.6 between the central Greece and the Peloponnese.

almost vertical seismic rays, capable to of better constraining the focal depth, but this also involves high residual times variance. This minimum in the hypocentral depth error is probably a trade-off between these two effects. The best-covered area is at about 350 km of the vertical section coinciding with the region between the central Greece and the Peloponnese. For this part of the vertical section the hypocentral depth appear well constrained until about 160 km with minimum value of about 3 km. For the rest of the vertical section the hypocentral depth is not well constrained (maximum depth of about 60 km) and show a very high error. The RES has a minimum value of about 1.8 km for shallow earthquakes (hypocentral depth < 30 km) at about 350 km on the vertical section A–A′. From RES analysis, it follows that for this vertical section, only between 150 and 550 km the hypocentre is well constrain until a depth of about 160 km, while out of this range the hypocentral depth is well constrain only to depths of about 60 km.

The vertical section B–B′, like A–A′, shows that both latitude and longitude errors increase with the depth showing minimum values of about 1 km at altitude zero. The epicentres appear well constrained in depth until about 180 km, reaching for the latitude about 250 km at 400 km of the vertical section. For shallow earthquakes ($H < 50$ km), the hypocentral depth is well constrained for almost the whole B–B′ vertical section, but for deep earthquakes ($H > 50$ km), the hypocentral depth is well constraint only between 130 and 400 km and between 450 and 550 km of the vertical section with a maximum depth of about 160 km. The RES show a rather horizontal homogeneity with minimum value at about 15 km of depth, and maximum depth covered of about 200 km.

CONCLUSION

The establishment of a modern, dense seismological network in an area of high seismicity, like Greece, will provide abundant data (waveforms, accurate earthquake catalogues, etc) that will be extremely useful for the scientific community. This paper aims to inform the scientific community about the operation of this modern network and its promising capabilities.

For this reason we apply the SNES method to the HUSN, which monitors since 2007 seismicity in Greece territory. We constructed a map of the average power of noise in the frequency range 1 12 Hz, which allowed us to identify areas of greater (Volcanic Arc with maximum in the Crete Island) and lower (rest of Greece) background noise within the HUSN.

A statistical study of the residual times of *P* and *S* phases permitted us to determined an empirical law that links the variance of the residual times of the *P* and *S* phases to the hypocentral distance. Both *P* and *S* phases residual times show little non-zeros mean values that may be introduce systematic errors in hypocentre locations. Variance of *P* and *S* residual times assumes large values for great hypocentral distance (>500 km) reducing the quality of

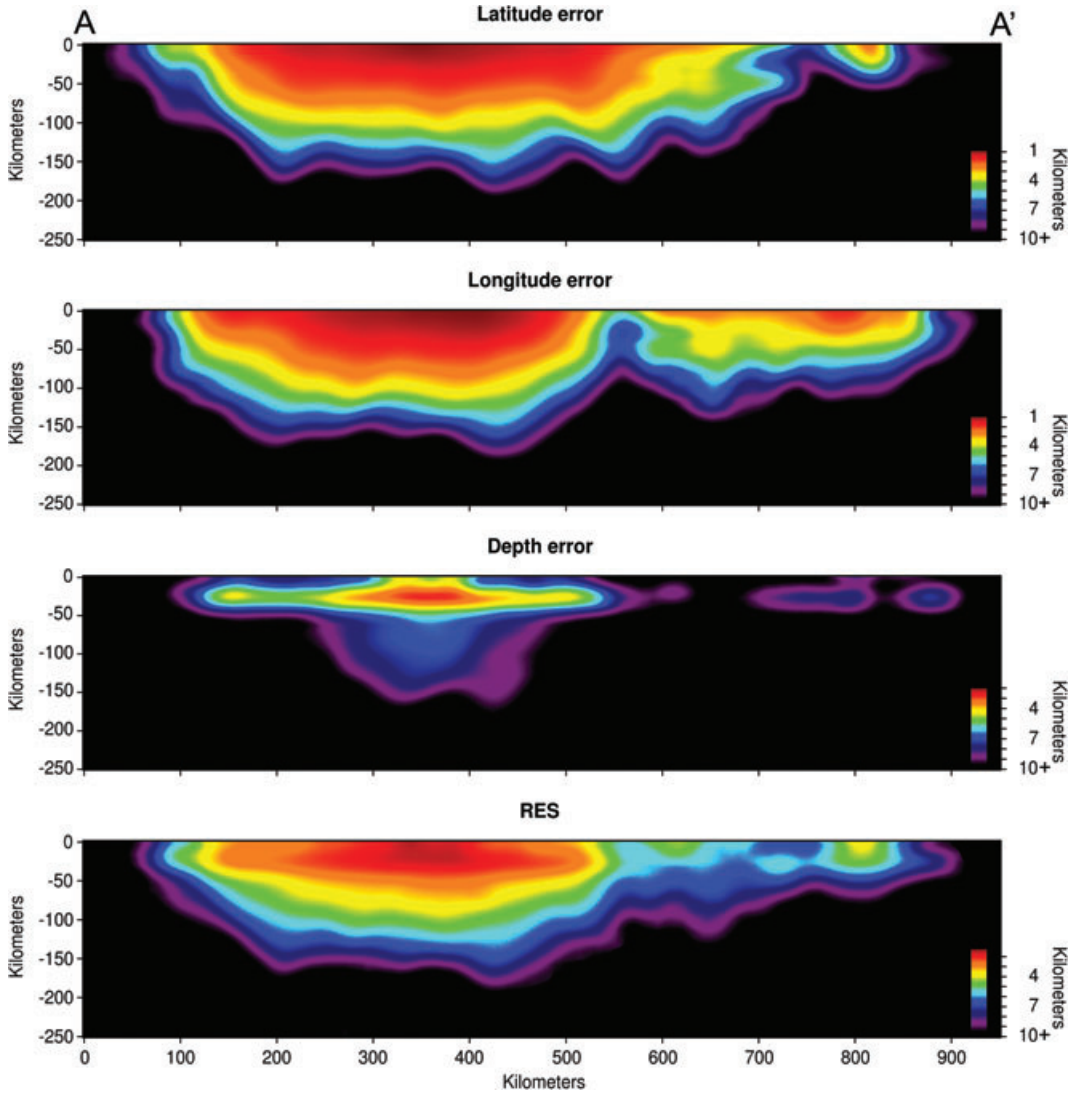

Figure 9. SNES vertical section between the points A (40.45N, 19.55E) and A′ (34.12N, 26.73E) (see Fig. 8), for $M_L = 2.5$ and confidence level of 95 per cent. For this magnitude the epicentres appear well constrained, above the hypocentral depth of about 160 km, for the western part of Greece and above about 120 km for the eastern part. The error in hypocentral depth shows a very variable value along the vertical section with a minimum value at a depth of about 25 km.

hypocentral location for distant earthquakes. A reduction of residual times can be achieved by using optimized velocity models for different regions of the Greek territory.

The SNES maps were constructed as function of the magnitude ($M_L = 2, 2.5, 3$), fixing the hypocentral depth to 10 km and the confidence level to 95 per cent. These maps show the spatial distribution of the number of active stations (in the hypocentral location process), the azimuthal gaps and relative amplitudes of the confidence interval of the hypocentral parameters.

For small magnitude earthquakes ($M_L = 2$) only two little areas in Macedonia and between the central Greece and Peloponnese are covered while for slightly larger magnitude earthquakes ($M_L = 2.5$) about the whole western Greek territory is covered with minimum RES value of about 2.5 km. For medium magnitude earthquake ($M_L = 3$) all Greece is well covered with minimum RES value of 2 km.

The M_C map shows that the whole Greek Territory is covered just for $M_L > 2$, with minimum magnitude of completeness of about 1.6 between the central Greece and the Peloponnese. This study has confirmed that the M_C is not a good measure of the performance of a seismic network. The main goal of a seismic network is to provide earthquake location with acceptable errors. The M_C do not provide any information about the expected error in hypocentre location. This parameter determines only if a seismic network is able to detect a seismic event; it not take into account the relative positions of the stations respect to the hypocentre and the errors introduced by the velocity model used in location routine. For this reasons the M_C tends to significantly overestimates the performance of a seismic network.

Through application of the SNES method, we show that for shallow earthquakes the HUSN provides the best monitoring coverage in the area between Central Greece and Peloponnese.

However, some areas, like Cyclades Islands, are not adequately covered by HUSN. For these areas the hypocentral depths show very high error values especially for deep earthquakes. The main reason of this large error is due to the low density of station in this offshore area. To improve the quality of location the HUSN need an offshore extension by the installation of some Ocean Bottom Seismometers.

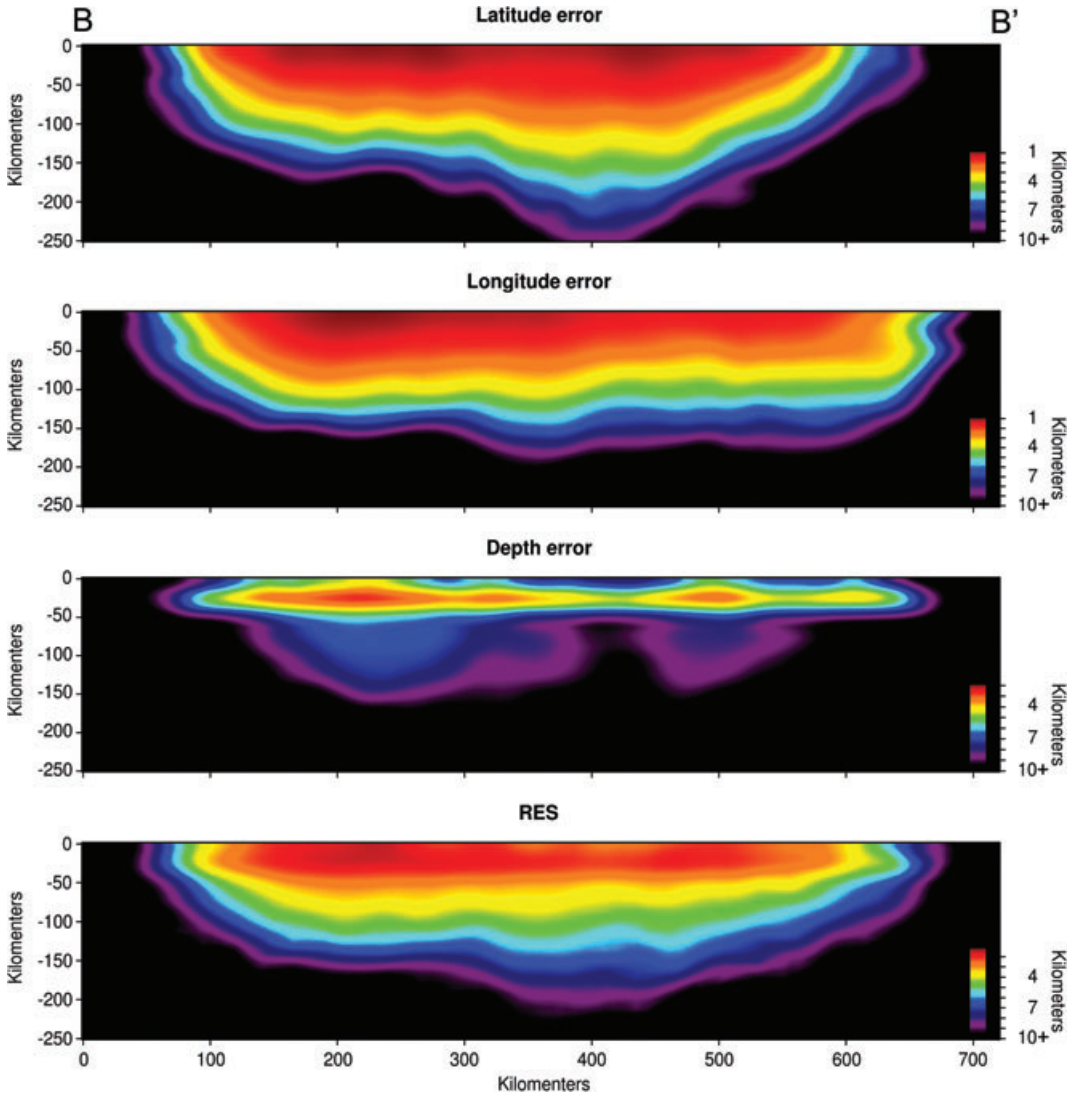

Figure 10. SNES vertical section between the points B (36.57N, 20.95E) and B′ (42.42N, 24.60E) (see Fig. 8), for $M_L = 2.5$ and confidence level of 95 per cent. The epicentres appear well constrained in depth above about 180 km. For shallow earthquakes ($H < 50$ km), the hypocentral depth is well constrained for almost the whole B–B′ vertical section.

The SNES technique can provides guidance for optimal upgrading to the network to provide adequate monitoring coverage for Greek seismogenic areas.

DATA AND RESOURCES

All data used in this paper came from the Institute of Geodymamics, National Observatory of Athens (Greece) and are available on http://bbnet.gein.noa.gr more information can be found in the following websites http://dggsl.geol.uoa.gr, http://geophysics.geo.auth.gr/ss/ and http://seismo.geology.upatras.gr belonging to the Seismological Laboratories of the Univesities of Athens, Thessaloniki and Patras, respectively.

ACKNOWLEDGMENTS

We are grateful to the two anonymous reviewers and associated editor for their constructive comments and suggestions.

REFERENCES

Amorèse, D., 2007. Applying a change-point detection method on frequency-magnitude distributions, *Bull. seism. Soc. Am.,* **97,** 1742–1749.

Anderson, J.G. & Hough, S.E., 1984. A model for the shape of the Fourier amplitude spectrum of acceleration at high frequencies, *Bull. seism. Soc. Am.,* **74**(5), 1969–1993.

Baskoutas, I., 1996. Dependence of Coda attenuation on frequency and lapse time in central Greece, *PAGEOPH,* **147**(3), 483–496.

Bohnhoff, M., Rische, M., Meier, T., Becker, D., Stavrakakis, G. & Harjes, H.-P., 2006. Microseismic activity in the Hellenic Volcanic Arc, Greece, with emphasis on the seismotectonic setting of the Santorini–Amorgos zone, *Tectonophysics,* **423,** 17–33.

Brocher, T.M., 2005. Empirical relations between elastic wavespeeds and density in the Earth's crust, *Bull. seism. Soc. Am.,* **95**(6), 2081–2092.

Brune, J.N., 1970. Tectonic stress and the spectra of seismic shear waves from earthquakes, *J. geophys. Res.,* **75,** 4997–5009.

Cao, A.M. & Gao, S.S., 2002. Temporal variation of seismic b-values beneath northeastern Japan island arc, *Geophys. Res. Lett.,* **29**(9), doi 10.1029/2001GL013775.

Comninakis, P.E. & Papazachos, B.C., 1972. Seismicity of the Eastern Mediterranean and some tectonic features of the Mediterranean ridge, *Bull. Geol. Soc. Am.,* **83,** 1093–1102.

D'Alessandro, A., Luzio, D., D'Anna, G. & Mangano, G., 2011. Seismic Network Evaluation through simulation: an application to the Italian National Seismic Network, *Bull. seism. Soc. Am.,* **101**(3), (in press).

Dewey, J.F. & Sengor, A.M.C., 1979. Aegean and surrounding regions: complex multiplate and continous tectonics in a convergent zone, *Bull. Geol. Soc. Am.,* **90,** 84–92.

Gomberg, J., 1991. Seismicity and detection/location threshold in the southern Great Basin seismic network, *J. geophys. Res.,* **96,** 16 401–16 414.

Hatzfeld, D., Besnard, M., Makropoulos, K. & Hatzidimitiou, P., 1993. Microearthquake seismicity and fault-plane solutions in the southern Aegean and its geodymanic implications, *Geophys. J. Int.,* **115,** 799–818.

Hatzidimitriou, P.M., 1993. Attenuation of Coda waves in Northern Greece, *PAGEOPH,* **140**(1), 63–78.

Herrin, E., Tucker, W., Taggart, J.N. & Lobdell, J.L., 1968. Estimation of surface focus travel times, *BSSA,* **58,** 1273–1292.

Karagianni, E.E. *et al*., 2002. Rayleigh wave group velocity tomography in the Aegean area, *Tectonophysics,* **358,** 187–209.

Karagianni, E.E., Papazachos, C.B., Panagiotopoulos, D.G., Suhadolc, P., Yuan, A. & Panza, G.F., 2005. Shear velocity structure in the Aegean area obtained by inversion of Rayleigh waves, *Geophys. J. Int.,* **160,** 127–143.

Kvaerna, T., Ringdal, F., Schweitzer, J. & Taylor, L., 2002. Optimized seismic threshold monitoring – part 1: regional processing, *PAGEOPH* **159**(5), 969–987.

Makris, J., 1973. Some geophysical aspects of the evolution of the Hellenides, *Bull. Geol. Soc. Greece,* **10,** 206–213.

Makropoulos, K.C. & Burton, P.W., 1984. Greek tectonics and seismicity, *Tectonophysics,* **106,** 275–304.

Marsan, D., 2003. Triggering of seismicity at short timescales following California earthquakes, *J. geophys. Res.,* **108**(B5), 2266.

McCreery, C.S., Duennebier, F.K. & Sutton, G.H., 1993. Correlation of deep ocean noise (0.4–20 Hz) with wind, and the Holu spectrum a worldwide constant, *J. acoust. Soc. Am.,* **93,** 2639–2648.

McKenzie, D., 1978. Active tectonics of the Alpine-Himalayan belt: the Aegean Sea and surrounding regions, *Geophys. J. R. astron. Soc.,* **55,** 217–254.

McNamara, D.E. & Buland, R.P., 2004. Ambient noise levels in the Continental United States, *Bull. seism. Soc. Am.,* **94,** 1517–1527.

Mercier, J., 1977. Principal results of a neotectonic study of the Aegean Arc and its location within the Eastern Mediterranean, in *Proceedings of the VI Coll. Geol. Aegean Region, IGMR,* Athens, Greece, Vol. 3, pp. 1281–1291.

Papaioannou, Ch.A. & Papazachos, B.C., 2000. Time-independent and time-dependent seismic hazard in Greece based on seismogenic sources, *Bull. Seism. soc. Am.,* **90**(1), 22–33.

Papanastassiou, D., 1989. Detectability and accuracy on the determination of earthquake parameters of the seismological networks of the Institute of Geodynamics, National Observatory of Athens, *PhD thesis*. University of Athens, 225 p.

Papanastassiou, D., 2011. Detection-location capability of the Hellenic Unified Seismological Network (HUSN) operating by the Institute of Geodynamics, National Observatory of Athens, *Hellenic J. Geosci,* **45,** 209–216.

Papazachos, B.C., 1990. Seismicity of the Aegean and surrounding area, *Tectonophysics,* **178,** 287–308.

Papazachos, B.C. & Comninakis, P.E., 1971. Geophysical and tectonic features of the Aegean Arc, *J. geophys. Res.,* **76,** 8517–8533.

Peterson, J., 1993. Observation and modelling of background seismic noise. U.S. Geol. Surv. Open-File Rept., Albuquerque, 93–322.

Polatidis, A., Kiratzi, A., Hatzidimitriou, P. & Margaris, B., 2003. Attenuation of shear-waves in the back-arc region of the Hellenic arc for frequencies from 0.6 to 16 Hz, *Tectonophysics,* **367,** 29–40.

Rothman, R.L., Greenfield, R.J. & Hardy, H.H., 1974. Errors in hypocenter location due to velocity anisotropy, *Bull. seism. Soc. Am.,* **64,** 1993–1996.

Rydelek, P.A. & Sacks, I.S., 1989. Testing the completeness of earthquake catalogues and the hypothesis of self-similarity, *Nature,* **337,** 251–253.

Sato, H., Fehler, M. & Wu, R., 2002. Scattering and attenuation in of seismic wave in the lithosphere, in *International Handbook of Earthquake & Seismology part A,* eds Lee, W., Kanamori, H., Jennings, P., Kisslinger, H., ISBN 0124406521.

Schorlemmer, D. & Woessner, J., 2008. Probability of detecting an earthquake, *Bull. seism. Soc. Am.,* **98**(5), 2103–2117.

Sereno, T.J. Jr. & Bratt, S.R., 1989. Seismic detection capability at NORESS and implications for the detection threshold of a hypothetical network in the Soviet Union, *J. geophys. Res.,* **94**(B8), 10 397–10 414.

Shepard, D., 1968. A two-dimensional interpolation function for irregularly-spaced data, in *Proceedings of the 1968 23rd ACM National Conference,* New York, NY, pp. 517–524.

Soloviev, S.L., Karakaisis, G.F., Kovachev, S.A., Kuzin, I.P., Shoda, O.Y. & Tassos, S.T., 1992. Microearthquake hypocenter determination in the southern Aegean Sea from records of sea-floor and land-based seismographs, *Phys. Earth planet. Inter.,* **75,** 177–183.

Tsapanos, T.M., 2008. Seismicity and seismic hazard assesment in Greece, in *Proceedings of the NATO Advanced Research Workshop on Earthquake Monitoring and Seismic Hazard Mitigation in Balkan Countries,* Borovetz, Bulgaria, 11–18 September 2005, Series: NATO Science Series: IV: Earth and Environmental Sciences,Vol. 81, eds Husebye, E. S., XVIII, 289 p., ISBN: 978-1-4020-6813-3.

Tsapanos, T.M., Mäntyniemi, P. & Kijko, A., 2004. A probabilistic seismic hazard assessment for Greece and the surrounding region including site-specific considerations, *Ann. Geophys.,* **47**(6), 1675–1688.

Wiemer, S. & Wyss, M., 2000. Minimum magnitude of complete reporting in earthquake catalogs: examples from Alaska, the Western United States, and Japan, *Bull. seism. Soc. Am.,* **90,** 859–869.

Woessner, J. & Wiemer, S., 2005. Assessing the quality of earthquake catalogs: estimating the magnitude of completeness and its uncertainties, *Bull. seism. Soc. Am.,* **95**(4), 684–698.

Zeiler, C. & Velasco, A.A., 2009. Seismogram picking error from analyst review (SPEAR): single-analyst and institution analysis, *Bull. seism. Soc. Am.,* **99**(5), 2759–2770.